ORIGINAL PAPER

S-rich apatite-hosted glass inclusions in xenoliths from La Palma: constraints on the volatile partitioning in evolved alkaline magmas

Fleurice Parat · François Holtz · Andreas Klügel

Abstract The composition of S-rich apatite, of volatile-rich glass inclusions in apatite, and of interstitial glasses in alkaline xenoliths from the 1949 basanite eruption in La Palma has been investigated to constrain the partitioning of volatiles between apatite and alkali-rich melts. The xenoliths are interpreted as cumulates from alkaline La Palma magmas. Apatite contains up to 0.89 wt% SO_3 (3560 ppm S), 0.31 wt% Cl, and 0.66 wt% Ce_2O_3. Sulfur is incorporated in apatite via several independent exchange reactions involving (P^{5+}, Ca^{2+}) vs. (S^{6+}, Si^{4+}, Na^+, and Ce^{3+}). The concentration of halogens in phonolitic to trachytic glasses ranges from 0.15 to 0.44 wt% for Cl and from <0.07 to 0.65 wt% for F. The sulfur concentration in the glasses ranges from 0.06 to 0.23 wt% SO_3 (sulfate-saturated systems). The chlorine partition coefficients ($D_{Cl}^{apatite/glass}$) range from 0.4 to 1.3 (average $D_{Cl}^{apatite/glass} = 0.8$), in good agreement with the results of experimental data in mafic and rhyolitic system with low Cl concentrations. With increasing F in glass inclusions $D_F^{apatite/glass}$ decreases from 35 to 3. However, most of our data display a high partition coefficient (~ 30) close to $D_F^{apatite/glass}$ determined experimentally in felsic rock. $D_S^{apatite/glass}$ decreases from 9.1 to 2.9 with increasing SO_3 in glass inclusions. The combination of natural and experimental data reveals that the S partition coefficient tends toward a value of 2 for high S content in the glass (>0.2 wt% SO_3). $D_S^{apatite/glass}$ is only slightly dependent on the melt composition and can be expressed as: SO_3 apatite (wt%) $= 0.157 * \ln SO_3$ glass (wt%) $+ 0.9834$. The phonolitic compositions of glass inclusions in amphibole and haüyne are very similar to evolved melts erupted on La Palma. The lower sulfur content and the higher Cl content in the phonolitic melt compared to basaltic magmas erupted in La Palma suggest that during magma evolution the crystallization of haüyne and pyrrhotite probably buffered the sulfur content of the melt, whereas the evolution of Cl concentration reflects an incompatible behavior. Trachytic compositions similar to those of the (water-rich) glass inclusions analyzed in apatite and clinopyroxene are not found as erupted products. These compositions are interpreted to be formed by the reaction between water-rich phonolitic melt and peridotite wall-rock.

Keywords Apatite · Glass inclusion · Sulfur · Halogen · Partition coefficient · Phonolite · La Palma

Communicated by J. Hoefs.

F. Parat
Institut für Geowissenschaften, Mineralogie-Geochemie, Albertstraße 23b, 79104 Freiburg, Germany

F. Parat (✉)
Géosciences Montpellier, Université Montpellier 2, Place E. Bataillon, 34095 Montpellier, France
e-mail: Fleurice.Parat@gm.univ-montp2.fr

F. Holtz
Institut für Mineralogie, Universität Hannover, Callinstrasse 3, 30167 Hannover, Germany

A. Klügel
Universität Bremen, Fachbereich Geowissenschaften, 28334 Bremen, Germany

Introduction

Water is the most abundant volatile in magmas followed by carbon dioxide, sulfur, chlorine, fluorine, nitrogen, and noble gases. Although available data allow the evaluation of the behavior of H_2O and CO_2 in systems under magmatic conditions (e.g., Dixon et al. 1995; Botcharnikov

et al. 2006), accurate models for tracing the evolution of sulfur and halogen contents in magmatic system (pre-eruptive concentrations) are scarce. In addition, variations of the concentrations of S and Cl are difficult to interpret, because of the large number of interrelated intensive and extensive variables (e.g., pressure, temperature, glass composition, volatile fugacity) that can affect solubility behavior and partitioning (e.g., Carroll and Webster 1994; Botcharnikov et al. 2004; Burgisser and Scaillet 2007; Parat et al. 2008).

Volatiles are carried by magmas as dissolved species in silicate melt, as major components of fluid phases, or as constituents of minerals. Because silicate melts suffer degassing during ascent and because the released fluid phases are difficult to quantify (only possible for gas emissions with open-path FTIR, e.g., Burton et al. 2007), the determination of the compositions of glass inclusions and of volatile-bearing minerals are the only ways to address the question of volatile concentrations in magmas at depth. Glass inclusions may be scarce in volcanic and plutonic rocks, and volatile diffusion and/or post-entrapment crystallization may occur during cooling leading to possible under- or over-estimation of the volatile contents. In most magmatic systems, apatite is the best mineral that can provide information on volatile concentrations in melts, because sulfur, chlorine, and fluorine can be incorporated in apatite (in addition to OH groups). Although the F and Cl concentrations in apatite may re-equilibrate with surrounding melt within a relatively small time interval, the diffusivity of these halogens in apatite remains several orders of magnitude lower than that in silicate melts (at least 3 orders of magnitude; Dowty 1980; Brenan 1994; Balcone-Boissard et al. 2009). Thus, at least in volcanic eruptive products, the volatile contents in apatites may be used as proxies for volatile concentrations in the host magmas (Piccoli and Candela 2002). Furthermore, sulfur and halogen zoning in apatite may retain information about sulfide and sulfate crystallization, changes in volatile fugacities (e.g., due to magma recharge), and volatile saturation and exsolution during magmatic differentiation. Apatite is thus an excellent tracer of volatile evolution in magmas, provided that the partitioning of S, Cl, and F between apatite and silicate melt is known (e.g., Piccoli and Candela 1994; Streck and Dilles 1998; Boyce and Hervig 2009).

Two approaches may constrain the partitioning of volatiles between apatite and silicate melt: (1) analysis of natural apatites hosting glass inclusions, and (2) experimental approaches. In this paper, we analyzed S-rich fluorapatite and volatile-rich glass inclusions from alkaline gabbro xenoliths present in basanite lavas from the 1949 La Palma eruption, Canary Islands. The data are used to determine the partition coefficients of S, Cl, and F between

apatite and phonolitic and trachytic melt and to estimate the volatile solubility in sulfate-saturated phonolitic and trachytic melt. They are also used to test experimental data predicting the partition coefficient of volatiles between apatite and silicate melts. Finally, the pre-eruptive volatile contents and magma evolution beneath La Palma volcano are discussed using the analysis of glass inclusions in apatite as well as in clinopyroxene, amphibole, haüyne, and magnetite.

La Palma Alkaline gabbro xenoliths

The investigated alkaline gabbro xenoliths were ejected by the late 1949 basanite rift zone eruption from the Cumbre Vieja on La Palma (Klügel et al. 1999). They consist of brown interstitial glass and phenocrysts of clinopyroxene (10–40 vol.%, Mg# = 100*Mg/(Mg + Fe_total) = 55–77), amphibole (up to 45 vol.%, Mg# = 50–68), plagioclase (6–75 vol.%, An_{30-53}), haüyne (1–10 vol.%), titanite (1–4 vol.%), magnetite (2–4 vol.%; $X_{ülvo}$ = 28–36), apatite (up to 3 vol.%), and pyrrhotite (up to 1 vol.%, N_{FeS} = 0.90–0.87) (Fig. 1). Plagioclase and haüyne were the last phases to crystallize, and poikilitically enclose the other minerals in some samples. The texture, mineralogical composition, and whole-rock geochemistry of the xenoliths indicate that they are cumulates from alkaline La Palma magmas; the alkaline gabbros thus differ from the MORB-type gabbro xenoliths from the Jurassic oceanic crust also carried by the late 1949 lavas (Schmincke et al. 1998; Neumann et al. 2000). The presence of CO_2-dominated fluid inclusions in xenoliths and basanite phenocrysts
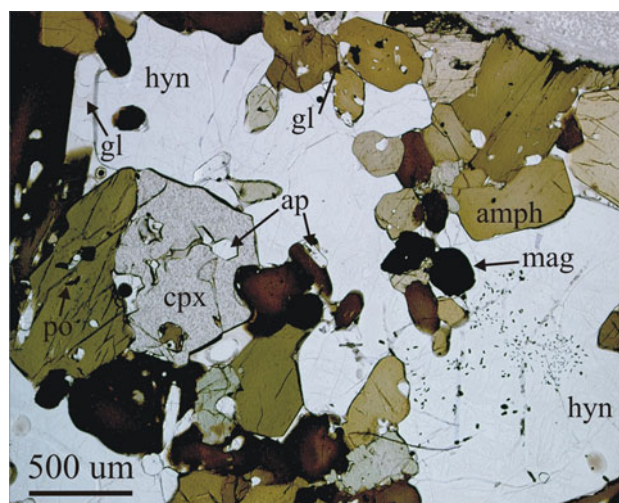

Fig. 1 Photomicrograph of alkaline gabbros from La Palma. *amph* amphibole, *cpx* clinopyroxene, *hyn* haüyne, *ap* apatite, *mag* magnetite, *po* pyrrhotite, *gl* glass

indicates fluid-saturated conditions at mantle depths (Hansteen et al. 1998).

The presence of S-rich apatite as inclusions in all silicate phases and oxides, and as interstitial minerals together with haüyne + pyrrhotite indicates that alkaline magmas of La Palma were sulfur-rich and relatively oxidized above the NNO buffer. This oxidation state agrees with estimates for the host basanite based on the Fe_2O_3/FeO ratio (NNO to NNO + 1.85; expressed as $\Delta \log fO_2$) (Klügel et al. 2000). Using the experimental calibration from Toulmin and Barton (1964), the composition of pyrrhotite ($N_{FeS} = 0.90–0.87$) indicates low sulfur fugacity with $\log fS_2 = 0.6$ to 1.7 (<50 bar) for $T = 900°C$ (apatite saturation temperature; Piccoli and Candela 1994).

Analytical procedure

Electron microprobe

The composition of minerals and glasses was determined by electron microprobe at the University of Freiburg using a Cameca Camebax SX100 electron microprobe operating at 15 keV accelerating voltage and 20 nA for minerals and 10 nA for glasses. The electron beam was defocused to 5 to 15 μm diameter for glass analyses (15 μm for large glass inclusions and interstitial glass), and 2–3 μm diameter electron beam for mineral analyses. Counting times on peak were 20 s for major elements and 60 s for F, Cl, and S. Volatiles and Na_2O were analyzed in the first pass. For accurate F and Cl analyses of apatite, we followed the analytical method proposed by Webster et al. (2009b) and slightly moved the apatite (2–3 μm) under a defocused electron beam during analysis. We also checked for the evolution of F with time in apatite, and no variation was observed (in particular increase in F with time). Standards used for calibration were the following: albite (Na), wollastonite (Si, Ca (glass)), Durango apatite (Ca and F for apatite and P for glass and apatite), F-phlogopite (F for glass and amphibole), orthoclase (K), baryte (S for apatite, haüyne, and glass), pyrite (S for pyrrhotite), scapolite (Cl), Al_2O_3 (Al), Fe_2O_3 (Fe), MgO (Mg), rhodonite (Mn, Ti), and $CePO_4$ (Ce). The analytical precision (repeated analyses of a standard, 2σ) is better than 1 wt% for elements at concentrations greater than 1 wt% and 0.04% for trace elements. The standard deviations for volatiles are S < 0.04 wt%, Cl < 0.05 wt%, and F < 0.5 wt%; the detection limits are S = 140 ppm for apatite and 250 ppm for glass, Cl = 340 ppm, and F = 1000 ppm.

Volatile-bearing glass standards (S = 150–1200 ppm, F = 0.5 wt%, H_2O = 0.1–8 wt%) were analyzed several times during glass inclusion analyses to control volatile concentrations. The water content of glass inclusions was determined using the "by-difference" method (i.e., 100%—total microprobe analyses, Devine et al. 1995; Koepke 1997), and two sets of standard of hydrous andesitic and rhyolitic glasses with known water contents (0.1 to 8 wt% H_2O measured by Karl Fischer Titration analysis). Glass standards were analyzed during each electron microprobe session, and the obtained calibration curve was used to improve the analyses of the water content. Although analyses with Secondary Ion Mass Spectrometry (SIMS) or infrared spectroscopy (IR) may be more accurate, the analytical approach used in this paper has been tested in previous studies in which water concentrations in glasses were analyzed by microprobe and by other techniques (IR, Karl Fischer Titration). Based on the datasets obtained in all these previous examples (Botcharnikov et al. 2008; Parat et al. 2008), the typical error on water analyses determined by microprobe (using standards) is ±0.5 to 0.7 wt% H_2O. For the purpose of this study, this precision is sufficient for further interpretations.
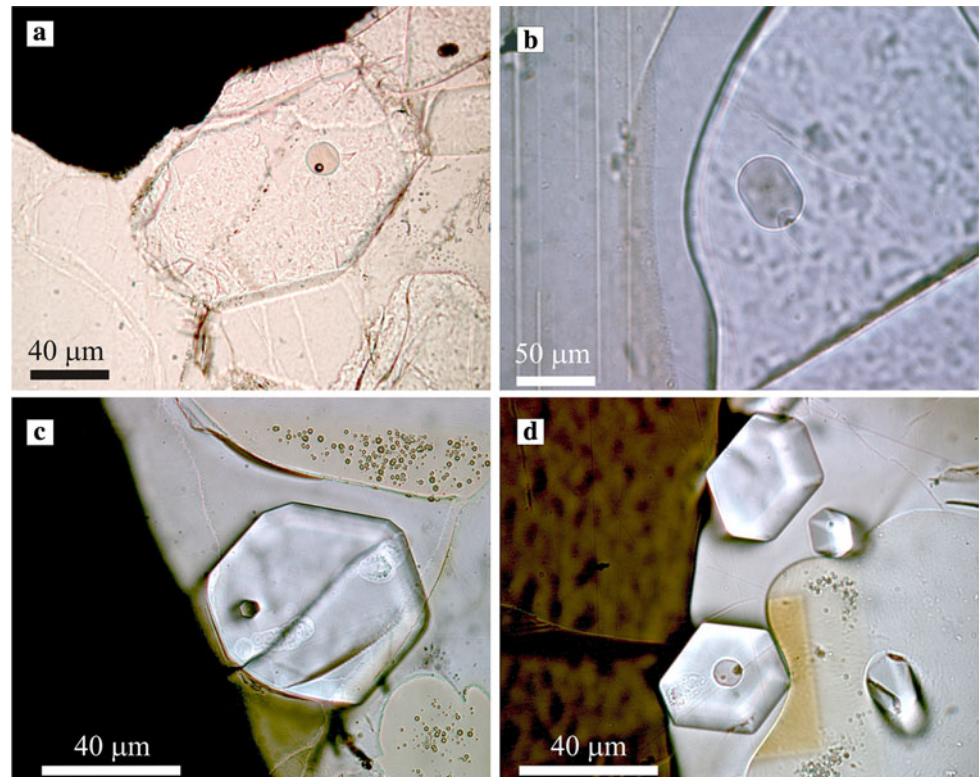
Sulfur speciation

A peak search was performed for S-Kα radiation for sulfur using a Large-PET crystal (2d = 8.75 Å), a beam current of 20 nA and a 10-μm spot. The mean peak position for S in apatite and the peak position of glass inclusions (one spot) were compared with the mean positions for four different spots measured on standards of pyrite (S^{2-}) and anhydrite (S^{6+}) and with the peak position of experimental glasses from runs performed at NNO + 2.6 (Parat and Holtz 2004). The difference in peak position between anhydrite and pyrite, $\Delta\lambda(S-K\alpha) = 1.3$ eV, is in agreement with the previous data on S peak search (compilation in Matthews et al. (1999)). Sulfur speciation was determined for natural glass inclusions using the equation proposed by Matthews et al. (1999).

Glass inclusions

Primary magmatic inclusions were identified in apatite as well as in clinopyroxene, magnetite, amphibole, and haüyne. They consist of pale brownish-colored silicate glass with or without small shrinkage/vapor bubble, randomly distributed in all host crystals (in core as well as rim) (Fig. 2). Glass inclusions in crystals without cracks or fractures were chosen for analyses. No post-entrapment crystallization was observed in the inclusions using backscattered electron (BSE) imagery. Thus, glass inclusions have been analyzed without pre-heating (note that Nikogosian et al. (2002) reported that even after pre-heating, full homogenization of bubble-bearing glass inclusions in olivine and clinopyroxene of La Palma was not achieved).

Fig. 2 Photomicrographs of apatite-hosted glass inclusion from alkali gabbros from La Palma (Canary Islands)

All inclusions show a spherical to ellipsoidal or a negative crystal shape (Fig. 2c) and range in size from 10 to 50 μm (Table 1). Among the 20 glass inclusions analyzed in apatite, 6 glass inclusions have apparent bubbles (<2.5 vol.%, assuming spherical glass inclusion and bubble). No vapor-rich phase (liquid) and no daughter minerals have been identified in bubbles. The absence of a separate vapor phase in the bubbles and the low bubble/glass ratios suggest that they formed by shrinkage upon quenching rather than being primary bubbles (hypersaline liquid or low density fluid) (Lowenstern 1995). However, because it cannot be ruled out that the bubbles contain a low-density fluid (e.g., $H_2O–CO_2$-fluid), the water content estimated for the host glass should be considered as a minimum value. Sulfur and chlorine are less volatile than CO_2, and they will not partition into low-density fluid. Furthermore, if a sulfur-rich fluid phase would have been present, we would expect sulfide- and/or sulfate crystals around the bubble (Kamenetsky et al. 2002). No differences in water, sulfur, and chlorine concentrations between bubble-bearing and bubble-free inclusions have been observed (note that some bubbles have been removed during thin-section preparation). Previous studies on glass inclusions from Vesuvius with shrinkage bubbles similar to those observed in this study reported the same range of volatile content in homogenized glass inclusions (Belkin et al. 1998) and unhomogenized glass inclusions (Vaggelli et al. 1993;

Marianelli et al. 1995), indicating that bubbles most probably do not contain sulfur and halogen.

Apatite and glass compositions

Apatite compositions

Apatite occurs as euhedral crystals (up to 300 μm) as inclusions in all silicate phases and magnetite or as interstitial crystals. They are fluorapatites with F and Cl concentrations ranging between 2.50 and 3.52 wt% F, and 0.17 and 0.31 wt% Cl, respectively (Cl/F = 0.07–0.11). The sulfur content in apatite ranges from 0.46 to 0.89 wt% SO_3 (Table 1). The peak positions for S in apatite are close to the mean peak position of anhydrite standard ($\Delta\lambda$(S-Kα) = 0.2–0.3 eV), suggesting that sulfur is incorporated as sulfate (S^{6+}) in apatite. All analyzed apatite crystals show an increase of the sulfur content from the core to the rim from 0.5–0.6 to 0.8–0.9 wt% SO_3, whereas F slightly decreases and Cl is constant.

No difference in composition has been observed between apatite as inclusions and interstitial apatites. The possible sulfate exchange reactions in apatite are shown in Fig. 3. In general, a colinearity of Na with S and of Si with S at an atomic ratio of one is consistent with the S exchange reactions $S^{6+} + Na^+ \Leftrightarrow P^{5+} + Ca^{2+}$ (Liu and

Table 1 Composition of glass inclusion and hosted apatite from La Palma alkaline gabbroic xenolith

Glass inclusion	GI 2	GI 4	GI 5	GI6	GI 8	GI 10	GI 11	GI 12	GI 14	GI 15	GI 16	GI 17	GI 18	GI 23a	GI 23b	GI 26	GI 27	GI 28	GI 29	GI 30
Size (μm)	10	30	7	35	15	10	10	10	15	15	10	10	25	12	10	10	15	20	20	15
Normalized to 100% anhydrous (wt%)																				
SiO_2	60.47	59.45	61.07	60.10	62.61	61.44	61.16	59.30	61.45	60.90	61.68	60.22	61.35	62.46	61.76	58.67	59.02	62.58	61.07	61.65
TiO_2	1.10	0.66	0.64	0.61	0.68	0.44	0.61	0.66	0.85	1.19	0.75	0.70	0.53	1.00	0.62	0.70	0.70	1.03	0.75	0.00
Al_2O_3	23.09	22.10	21.96	22.50	21.65	22.17	22.12	21.62	23.84	23.06	22.84	21.99	22.82	22.81	21.82	21.23	21.86	23.25	22.55	22.00
FeO_t	1.64	2.46	2.21	3.30	2.43	2.83	3.13	3.58	1.27	1.38	2.46	2.56	2.36	2.21	2.24	3.51	2.80	1.19	2.49	2.51
MnO	0.17	0.06	0.24	0.07	0.26	0.19	0.07	0.11	0.00	0.11	0.07	0.04	0.17	0.17	0.13	0.28	0.13	0.25	0.00	0.00
MgO	0.15	0.35	0.12	0.36	0.23	0.26	0.40	0.35	0.09	0.12	0.27	0.38	0.25	0.16	0.34	0.75	0.35	0.04	0.29	0.23
CaO	3.08	2.36	2.86	2.02	2.53	2.55	1.77	3.14	2.60	3.31	2.18	2.84	2.18	1.66	2.49	3.41	1.99	2.51	1.55	1.76
Na_2O	5.91	7.04	4.93	5.37	4.15	5.19	5.04	6.74	5.24	5.93	4.94	5.51	5.07	4.98	5.67	5.91	6.80	5.29	5.10	6.00
K_2O	3.71	4.88	4.28	4.64	3.80	4.11	5.02	3.91	3.26	2.76	4.21	4.76	4.60	3.83	3.97	4.99	5.75	3.12	5.16	5.29
P_2O_5	0.29	0.14	0.73	0.33	0.56	0.23	0.37	0.22	0.71	0.38	0.23	0.70	0.37	0.26	0.46	0.19	0.19	0.29	0.51	0.21
SO_3	0.13	0.11	0.13	0.06	0.15	0.15	0.10	0.11	0.23	0.14	0.10	0.10	0.08	0.16	0.14	0.06	0.12	0.11	0.11	0.11
S (ppm)	505	430	520	246	581	597	413	446	906	565	406	385	304	640	569	238	475	459	451	431
F	d.l.	0.07	0.52	0.31	0.65	0.17	d.l.	d.l.	0.10	0.28	d.l.	d.l.	d.l.	d.l.	0.07	0.12	d.l.	d.l.	0.14	0.08
Cl	0.26	0.30	0.32	0.33	0.30	0.27	0.21	0.26	0.35	0.44	0.26	0.20	0.22	0.29	0.28	0.19	0.29	0.34	0.29	0.15
H_2Oc	4.38	2.49	3.42	1.60	2.39	3.25	2.98	1.13	3.51	4.56	3.29	2.72	3.60	4.90	3.26	2.04	1.21	4.38	3.16	3.30
Total[a]	93.72	96.28	95.02	97.47	96.41	95.25	95.62	98.11	94.90	93.48	95.20	95.97	94.77	93.02	95.23	96.88	98.00	93.73	95.37	95.18
A/CNK	1.19	1.04	1.22	1.28	1.39	1.26	1.31	1.03	1.41	1.23	1.37	1.14	1.32	1.48	1.20	1.00	1.04	1.40	1.34	1.17
Mg#	14.3	20.2	9.1	16.1	14.3	14.2	18.5	15.0	11.5	13.6	16.6	21.1	15.8	11.6	21.5	27.7	18.3	5.1	17.2	14.2
Hosted apatite (wt%)																				
SiO_2	0.63	0.53	0.50	0.59	0.59	0.48	0.36	0.50	0.44	0.47	0.55	0.51	0.46	0.50	0.65	0.40	0.52	0.44	0.43	0.55
Al_2O_3	0.03	0.00	0.00	0.01	0.01	0.00	0.01	0.01	0.04	0.00	0.02	0.00	0.00	0.00	0.01	0.01	0.01	0.00	0.00	0.00
MnO	0.03	0.06	0.07	0.02	0.09	0.09	0.06	0.09	0.05	0.14	0.13	0.03	0.10	0.03	0.02	0.12	0.05	0.05	0.03	0.00
CaO	52.89	55.08	54.75	54.49	54.58	55.08	54.98	54.43	54.40	54.81	54.81	54.24	54.53	53.96	53.77	54.88	54.52	55.10	54.88	53.92
Na_2O	0.28	0.24	0.18	0.10	0.25	0.21	0.18	0.17	0.21	0.26	0.22	0.23	0.18	0.17	0.25	0.15	0.17	0.11	0.17	0.20
P_2O_5	39.61	40.69	39.81	40.74	40.14	40.60	41.46	40.38	41.67	42.11	41.40	41.28	40.08	41.20	42.29	41.94	41.54	41.85	41.11	41.96
SO_3	0.78	0.65	0.63	0.46	0.78	0.70	0.60	0.61	0.67	0.63	0.70	0.67	0.63	0.61	0.74	0.54	0.80	0.68	0.68	0.61
S (ppm)	3564	3295	2537	1855	3206	2812	2400	2443	2661	2521	2805	2673	2514	2460	3457	2175	3196	2732	2726	2455
Ce_2O_3	0.50	0.17	0.57	0.41	0.47	0.27	0.36	0.40	0.21	0.51	0.58	0.30	0.32	0.31	0.41	0.35	0.38	0.15	0.55	0.39
F	2.86	2.60	2.81	3.28	2.05	2.81	3.25	2.53	2.78	2.52	2.52	3.22	2.53	3.04	2.67	2.98	2.57	2.60	2.50	2.54
Cl	0.28	0.30	0.21	0.25	0.31	0.19	0.19	0.19	0.17	0.18	0.20	0.19	0.29	0.26	0.28	0.24	0.28	0.26	0.31	0.16
OHc	0.31	0.46	0.37	0.15	0.70	0.38	0.19	0.50	0.41	0.53	0.52	0.20	0.48	0.26	0.44	0.31	0.48	0.48	0.55	0.52
Total	97.90	100.33	99.53	100.34	99.27	100.44	101.16	99.31	100.65	101.65	101.14	100.66	99.13	100.08	101.08	101.62	100.86	101.25	100.67	100.93
O–F,Cl	1.27	1.16	1.23	1.44	0.93	1.23	1.41	1.11	1.21	1.10	1.11	1.40	1.13	1.34	1.19	1.31	1.14	1.15	1.12	1.11
XFap	0.76	0.69	0.75	0.87	0.54	0.75	0.86	0.67	0.74	0.67	0.67	0.85	0.67	0.81	0.71	0.79	0.68	0.69	0.66	0.67

Table 1 continued

Glass inclusion Size (µm)	GI 2 10	GI 4 30	GI 5 7	GI6 35	GI 8 15	GI 10 10	GI 11 10	GI 12 10	GI 14 15	GI 15 15	GI 16 10	GI 17 10	GI 18 25	GI 23a 12	GI 23b 10	GI 26 10	GI 27 15	GI 28 20	GI 29 20	GI 30 15
XClap	0.04	0.04	0.03	0.04	0.04	0.03	0.03	0.03	0.03	0.03	0.03	0.03	0.04	0.04	0.04	0.04	0.04	0.04	0.05	0.02
XOHap	0.20	0.27	0.22	0.09	0.41	0.23	0.11	0.30	0.24	0.30	0.30	0.12	0.29	0.16	0.25	0.17	0.28	0.27	0.29	0.30
$D_S^{apatite/melt}$	6.2	6.0	4.9	7.5	5.4	4.7	5.8	5.5	2.9	4.5	6.9	6.9	8.3	3.8	5.2	9.1	6.7	6.0	6.0	5.7
$D_{Cl}^{apatite/melt}$	1.1	1.0	0.7	0.8	1.0	0.7	0.9	0.7	0.5	0.4	0.8	0.9	1.3	0.9	1.0	1.2	1.0	0.8	1.1	1.0
$D_F^{apatite/melt}$	–	(37.1)	5.4	10.6	3.1	16.5	–	–	(27.8)	9.2	–	–	–	–	(38.1)	(24.8)	–	–	(17.6)	(31.8)

H_2Oc: water content determined by difference, using standards of rhyolitic glass with different water contents (0 to 8 wt% H_2O) following the method described by Devine et al. (1995) and Koepke (1997)

[a] Total microprobe. d.l.: below detection limit. A/CNK = Al_2O_3/(CaO + Na_2O + K_2O) molar. Mg# = $100 \times$ Mg/(Mg + Fet). XFap, XClap and XOHap calculated following Piccoli and Candela (2002). OH concentration in apatite (OHc) estimated assuming that the halogen site is filled by Cl, F and OH. D in brackets are ratio with data close or below detection limit
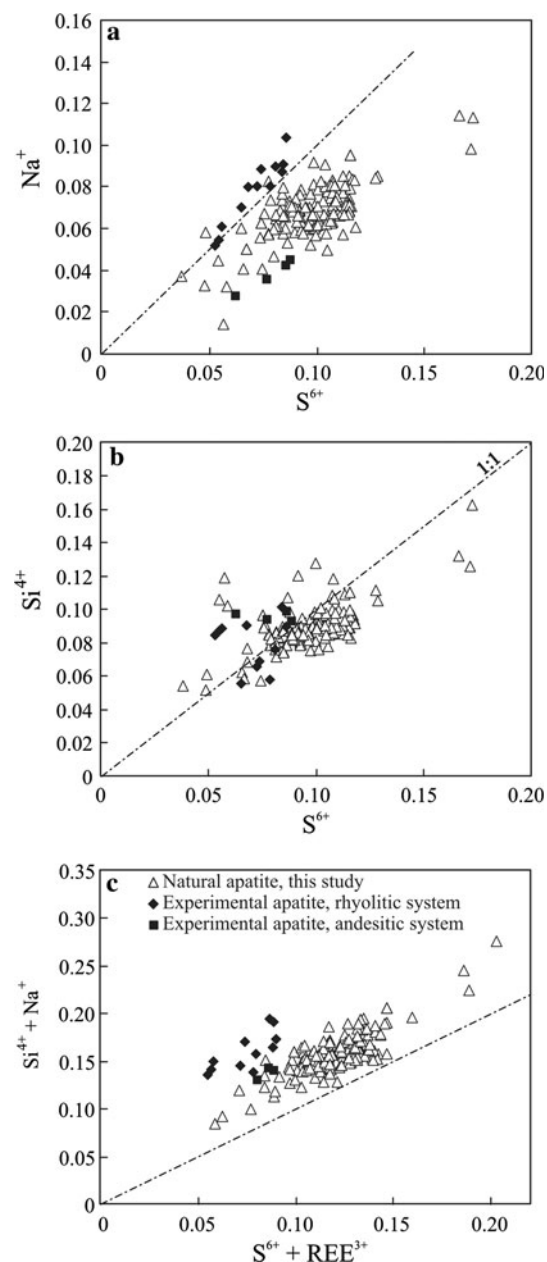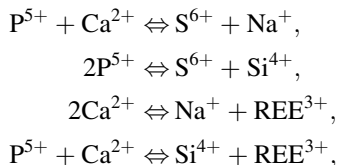

Fig. 3 Sulfate exchange reactions in apatite. **a** $P^{5+} + Ca^{2+} = S^{6+} + Na^+$ (Liu and Comodi 1993); **b** $2P^{5+} = S^{6+} + Si^{4+}$ (Rouse and Dunn 1982); **c** $2P^{5+} + 2Ca^{2+} = S^{6+} + Na^+ + Si^{4+} + REE^{3+}$ (Tepper and Kuehner 1999); $n = 140$. Apatite crystallization experiments with synthetic (REE-free) rhyolitic and natural andesitic composition from Parat and Holtz (2004, 2005) and Parat et al. (2008), respectively

Comodi 1993) and $S^{6+} + Si^{4+} \Leftrightarrow 2P^{5+}$ (Rouse and Dunn 1982). In REE- (rare earth elements) free systems, the sulfur exchange reaction proposed by Liu and Comodi (1993) was confirmed by experimental data from crystallization experiments (Parat and Holtz 2004; 2005). However, the nonzero intercept and the slope slightly higher than 1 in Fig. 3 suggest some influence of an additional

coupled exchange reaction in REE-bearing system (Parat et al. 2008). Tepper and Kuehner (1999) proposed an exchange involving REE: $2P^{5+} + 2Ca^{2+} \Leftrightarrow S^{6+} + Na^+ + Si^{4+} + REE^{3+}$. Such an exchange reaction may be useful to explain the apatite compositions from La Palma gabbros containing up to 0.66 wt% Ce_2O_3. However, Fig. 3c shows that the reaction proposed by Tepper and Kuehner (1999) cannot explain the natural compositions. The following independent substitution reactions probably explain most of the compositional variations observed in the apatite:

$$P^{5+} + Ca^{2+} \Leftrightarrow S^{6+} + Na^+,$$
$$2P^{5+} \Leftrightarrow S^{6+} + Si^{4+},$$
$$2Ca^{2+} \Leftrightarrow Na^+ + REE^{3+},$$
$$P^{5+} + Ca^{2+} \Leftrightarrow Si^{4+} + REE^{3+},$$

with the Ca-site accommodating large cations (e.g., Na^+, REE^{3+}) and P-site accommodating small highly charged cations (e.g., S^{6+}, Si^{4+}) (Piccoli and Candela 2002).

Glass inclusion and interstitial glass composition

Glass inclusions have a range in composition from phonolite to trachyte ($SiO_2 = 54$ to 63 wt% and $Na_2O + K_2O = 12$ to 8 wt%; Fig. 4 and Tables 1, 2). They represent an evolved metaluminous to peraluminous silicate glass (molar Al/(Ca + Na + K) = 0.8 to 1.5; (Na + K)/Al = 1.0 to 1.9, Fig. 5) contrasting with the less
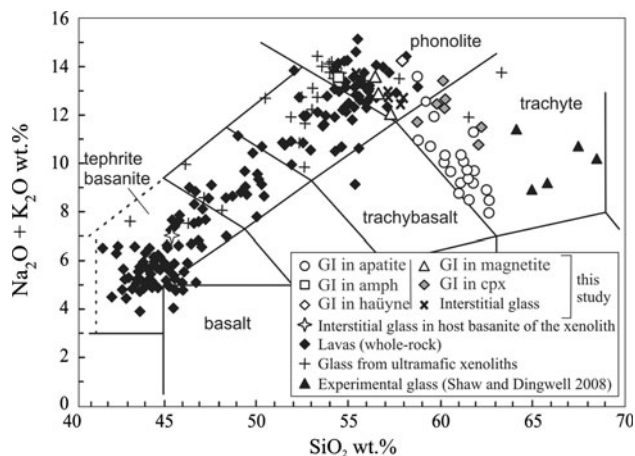

Fig. 4 Total alkali versus silica of Recent La Palma lavas, glass inclusions (GI), and interstitial glasses in xenoliths (amph-amphibole; cpx-clinopyroxene). Whole-rock compositions of lavas are from Klügel et al. (2000), Hernández-Pacheco and De La Nuez (1983), Hernández-Pacheco and Valls (1982), Middlemost (1972), Johansen et al. (2005), and Carracedo et al. (2001). Glass compositions from ultramafic xenoliths are from Wulff-Pedersen et al. (1996, 2000). Experimental glasses formed by reactions between peridotite and Si-undersaturated basaltic melts (Type 2) from Shaw and Dingwell (2008). All analyses are normalized to 100 wt% anhydrous

evolved interstitial melt composition of the host basanite of the xenoliths ($SiO_2 = 45.7$ wt%; $Na_2O + K_2O = 7$ wt%, molar (Na + K)/Al = 0.7) (Fig. 4). The molar Al/(Ca + Na + K) of the interstitial melt of the host basanite is 0.8 and overlaps with that of the evolved melt inclusions in the xenoliths. Haüyne, magnetite, and amphibole contain phonolitic glass inclusions ($SiO_2 = 54$–57 wt%), whereas the glass inclusions in clinopyroxene and apatite have trachytic compositions with a SiO_2 content ranging from 58 to 63 wt% (Fig. 4). The composition of the glass inclusions in the different minerals is coherent with a general differentiation trend (with increasing silica content, Al_2O_3 increases, and MgO and FeO decrease, Fig. 5). The interstitial glass composition is close to that of glass inclusions in amphibole, magnetite, and haüyne (Fig. 5). K_2O shows significantly less variation in clinopyroxene-hosted glass inclusions (4.99–5.61 wt%) than in apatite-hosted ones (2.76 to 5.75 wt%). For a given SiO_2 concentration, glass inclusions in clinopyroxene have slightly lower Al_2O_3 and CaO, and higher K_2O and Na_2O concentrations than glass inclusions in apatite.

It is conspicuous that CaO and P_2O_5 are higher in melt inclusions in apatite compared to those in other minerals for a given SiO_2 content (Fig. 5). This may be explained by biased analyses due to analytical artifacts (excitement of host apatite by the electron beam), post-entrapment processes (melting of host apatite), or kinetic effects during crystallization. However, these effects are of minor magnitude and should not affect our interpretations for the following reasons: (1) the higher concentrations in CaO and P_2O_5 are accompanied by higher Al_2O_3 and lower K_2O, Na_2O, and FeO concentrations (Fig. 5), which cannot be explained by apatite involvement; (2) there is no correlation between the size of an inclusion and its P_2O_5 content; (3) even if host apatite caused biased glass analyses, a simple mass balance shows that a contamination of ~ 1.2 wt% would be sufficient to increase P_2O_5 from 0.2 wt% to 0.7 wt% and CaO from 1.5 wt% to 2.1 wt%. This small contamination would not affect the concentrations of incompatible elements such as K_2O and would only slightly increase the analyzed volatile contents of glass inclusions (max 0.004, 0.004, and 0.04 wt% for S, Cl, and F, respectively; cf. Tables 1 and 2), with negligible effect on the calculated partition coefficients.

For other glass inclusions, only those in magnetite appear to be affected by analytical artifacts or minor post-entrapment melting of the host phase, as is suggested by their relatively high FeO concentrations. However, no correction to the data was carried out.

The total H_2O contents of the glass inclusions in apatite and clinopyroxene vary considerably from 1.1 to 4.9 wt% and 2.0 to 3.1 wt%, respectively. In contrast, glass inclusions in amphibole, magnetite, and interstitial glass have

Table 2 Composition of glass inclusion in minerals, hosted minerals, and interstitial glass from La Palma alkaline gabbroic xenolith

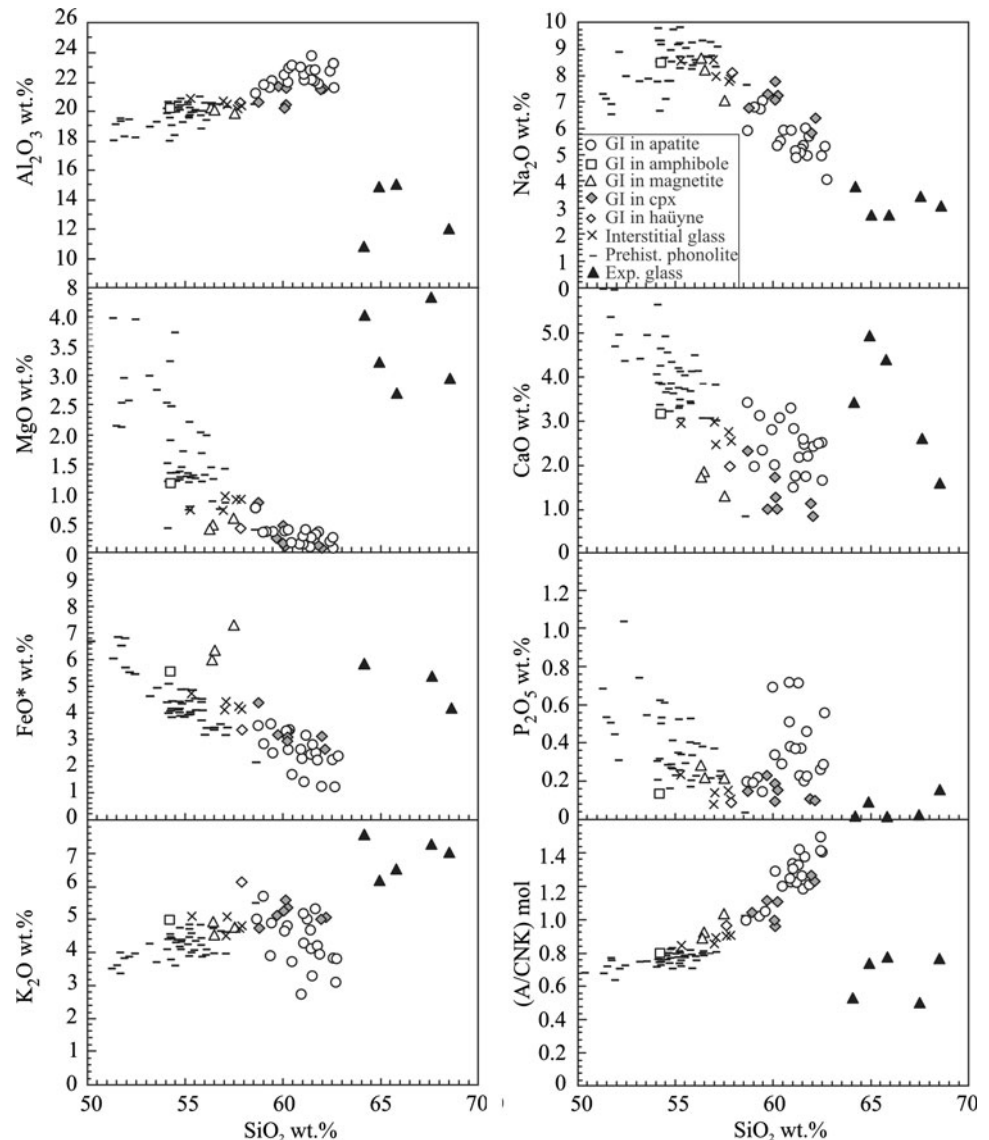| Glass Size (μm)	GI 26 120	GI 8 60	GI 16 20	GI 17 20	GI 24 60	GI 25 100	GI2 20	GI3 30	GI4 50	GI 28 60	GI 29 50	GI34 70	IG 12 Interst.	IG 13 Interst.	IG15 Interst.	IG18 Interst.	IG 22 Interst.
Normalized to 100% anhydrous (wt%)																	
SiO_2	57.84	54.22	59.70	60.21	60.07	60.07	62.08	61.93	58.72	56.31	56.45	57.50	57.73	57.84	57.07	56.99	55.28
TiO_2	0.66	1.45	0.90	0.77	0.59	0.81	0.73	0.75	0.83	0.82	0.97	0.67	0.90	0.88	1.02	0.80	0.96
Al_2O_3	20.60	20.17	21.72	21.64	20.56	20.27	21.52	21.53	20.60	20.19	20.12	19.85	20.30	20.42	20.43	20.77	20.97
FeOt	3.35	5.52	3.15	2.95	3.24	3.33	2.61	3.09	4.32	5.92	6.32	7.24	4.24	4.11	4.36	4.01	4.70
MnO	0.19	0.18	0.07	0.14	0.14	0.14	0.12	0.15	0.13	0.20	0.32	0.25	0.16	0.16	0.13	0.19	0.09
MgO	0.42	1.17	0.23	0.07	0.15	0.44	0.04	0.12	0.79	0.37	0.47	0.57	0.86	0.89	0.93	0.69	0.70
CaO	1.98	3.18	1.02	1.02	1.29	1.73	0.82	1.15	2.33	1.75	1.86	1.32	2.74	2.54	2.47	2.98	2.95
Na_2O	8.08	8.51	7.31	7.21	7.78	7.09	6.38	5.81	6.80	8.64	8.22	7.06	7.75	7.90	7.94	8.58	8.56
K_2O	6.16	5.05	5.14	5.35	5.61	5.25	5.05	4.99	4.75	4.91	4.59	4.78	4.70	4.78	5.09	4.52	5.07
P_2O_5	0.08	0.14	0.23	0.15	0.09	0.19	0.10	0.11	0.15	0.28	0.22	0.21	0.16	0.10	0.14	0.08	0.22
SO_3	0.23	0.02	0.24	0.11	0.07	0.20	0.13	0.11	0.25	0.15	0.11	0.12	0.07	0.03	0.11	0.05	0.10
S (ppm)	910	81	944	458	279	789	528	430	1013	609	422	481	278	130	433	203	408
F	0.11	0.11	0.10	0.11	0.12	0.16	0.17	0.09	0.07	0.14	0.13	0.16	0.15	0.13	0.11	0.14	0.18
Cl	0.30	0.29	0.21	0.25	0.28	0.32	0.35	0.26	0.27	0.32	0.23	0.26	0.23	0.21	0.20	0.20	0.22
H_2Oc	1.35	0.54	2.41	2.69	2.05	2.49	2.29	3.13	2.14	0.00	0.03	0.00	0.00	0.00	0.49	0.93	0.00
Total[a]	97.81	99.31	96.38	95.97	96.64	96.28	96.54	95.51	96.75	100.14	99.59	99.69	100.34	100.05	99.21	98.60	100.24
A/CNK	0.87	0.80	1.12	1.11	0.97	0.99	1.23	1.26	1.00	0.89	0.92	1.03	0.89	0.90	0.89	0.85	0.84
Mg#	18.2	27.4	11.5	4.2	7.5	19.0	2.8	6.4	24.6	10.1	11.6	12.3	26.6	27.9	27.6	23.4	21.0
Hosted mineral	haüyne	amph	cpx	cpx	cpx	cpx	cpx	cpx	cpx	mag	mag	mag					
SiO_2 (wt%)	33.89	37.99	47.89	49.02	48.32	47.69	49.27	46.96	47.20	0.05	0.04	0.04					
TiO_2	0.02	4.69	1.40	1.44	1.06	1.40	1.08	1.74	1.55	10.64	9.97	9.85					
Al_2O_3	28.11	13.69	4.98	4.62	4.26	4.61	4.20	6.19	4.44	2.27	2.01	2.02					
FeOt	0.07	14.83	11.43	11.10	12.01	12.00	12.47	11.67	12.30	77.66	78.28	79.26					
MnO	0.00	0.30	0.39	0.36	0.37	0.31	0.39	0.35	0.35	1.10	1.14	1.02					
MgO	0.02	10.10	9.85	10.55	9.66	10.11	9.93	9.71	9.90	1.47	1.40	1.45					
CaO	7.99	11.29	21.66	21.70	21.24	21.38	21.09	21.59	21.20	0.01	0.00	0.00					
Na_2O	16.62	2.78	1.64	1.54	1.65	1.48	1.84	1.43	1.53	0.00	0.02	0.07					
K_2O	0.91	1.24	0.00	0.00	0.02	0.00	0.01	0.00	0.00	0.01	0.00	0.00					
P_2O_5	0.08	0.03	0.01	0.00	0.02	0.00	0.07	0.01	0.00	0.05	0.00	0.05					
SO_3	12.24	0.00	0.00	0.00	0.00	0.00	0.01	0.01	0.00	0.00	0.00	0.00					
S ppm	48951	0	0	0	0	0	50	50	0	0	0	0					
F	0.04	0.24	0.06	0.05	0.05	0.06	0.07	0.05	0.06	0.13	0.15	0.12					
Cl	0.71	0.02	0.00	0.01	0.00	0.01	0.00	0.00	0.01	0.00	0.00	0.00					
Total	100.68	97.20	99.31	100.39	98.66	99.05	100.43	99.71	98.54	93.39	93.01	93.88					
Mg#		54.8	60.6	62.9	58.9	60.0	58.7	59.7	58.9								
DFet/Mg		0.31	0.08	0.03	0.06	0.16	0.02	0.05	0.23								
Xulv										32.0	30.0	29.0					

H_2Oc: water content determined by difference, using standards of rhyolitic glass with different water contents (0 to 8 wt% H_2O) following the method described by Devine et al. (1995) and Koepke (1997). [a]Total microprobe. A/CNK = $Al_2O_3/(CaO + Na_2O + K_2O)$ molar. Mg# = $100 \times Mg/(Mg + Fet)$, Xulv calculated according to Stormer (1983); amph: amphibole, cpx: clinopyroxene, mag: magnetite, interst.: interstitial glass

H_2O contents lower than 0.8 wt%. There is an overall increase in H_2O content with the degree of differentiation (e.g., SiO_2, Fig. 6). Post-entrapment crystallization of minerals appears to have been negligible in all investigated samples, and the high H_2O concentrations in apatite and clinopyroxene most probably represent H_2O content at the

time of host mineral crystallization at depth. Because volume and grain boundary diffusion in the host minerals may have affected (lowered) the initial water content of the glass inclusions (Portnyagin et al. 2008), and because magmatic amphiboles are not in equilibrium with melts containing less than 0.8 wt% H_2O, the estimated H_2O

Fig. 5 Composition of glass inclusions (GI) hosted by apatite, clinopyroxene (cpx), amphibole, haüyne, and magnetite and composition of interstitial glass from alkaline gabbroic xenolith from La Palma. Prehistoric phonolites from Hernandéz-Pacheco and De La Nuez ([1983]). Experimental glasses formed by reactions between peridotite and Si-undersaturated basaltic melts (Type 2) from Shaw and Dingwell ([2008]). All analyses are normalized to 100 wt% anhydrous

concentrations should be considered as minimum values, especially in amphibole (Luhr [2001]; Cervantes and Wallace [2003]; Streck and Wacaster [2006]). On the other hand, the positive correlation between SiO_2 and H_2O of trachytic melt inclusions in apatite and clinopyroxene (Fig. [6]) is interpreted to reflect evolutions at magmatic conditions rather than an analytical artifact, because the analytical uncertainty for SiO_2 is significantly smaller than the H_2O variation.

The sulfur concentration ranges from 0.02 to 0.25 wt% SO_3 (80 to 1010 ppm S; Tables [1], [2]). There is no clear correlation of the sulfur content with SiO_2 content (Fig. [6]) or with FeO, Na_2O, and CaO content which could have been expected as a result of pyrrhotite, haüyne, and anhydrite crystallization. The sulfur content roughly increases with increasing CaO/Al_2O_3 and Mg#. The highest values are observed for glass inclusions in clinopyroxene.

The sulfur content in interstitial glass is close to or slightly lower than the sulfur content in glass inclusions in apatite, with concentrations up to 0.11 wt% SO_3. We observed no evident correlation between SO_3 and H_2O content (Fig. [7]). The highest value in glass inclusions in apatite ($SO_{3\ glass}$ = 0.23 wt%) corresponds to the experimentally derived S solubility for water- and sulfide-sulfate-saturated glasses at 950–900°C for andesitic to trachyandesitic compositions containing 3.1 wt% and 1.9 wt% FeO_t, respectively (Luhr [1990]; Parat et al. [2008]) (Fig. [7]).

Sulfur peak search has been performed for the largest glass inclusions and interstitial glass. The peak positions are very close to the mean peak position of anhydrite standard ($\Delta\lambda(S-K\alpha)_{anh}$ = 0.06 to 0.40 eV), suggesting that sulfur was present mainly as S^{6+} at the time of glass inclusion entrapment and at the time of eruption. Using the calibration defined by Matthews et al. ([1999]), silicate
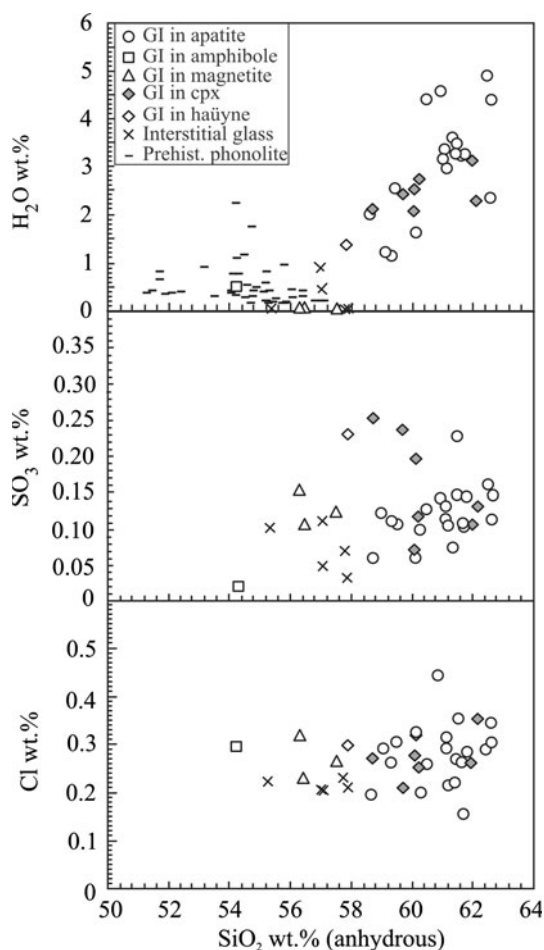
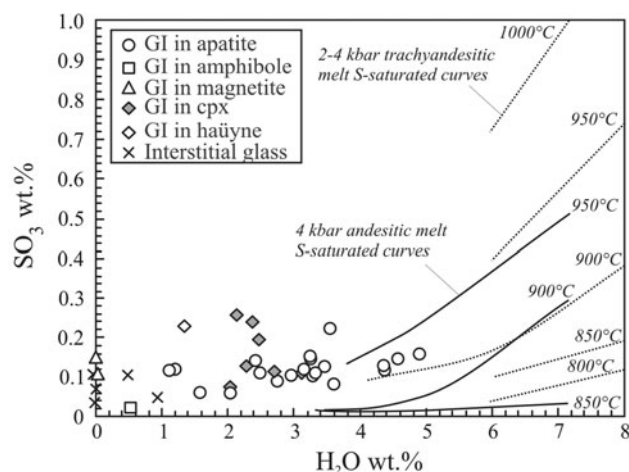**Fig. 6** Volatile content of glass inclusions (GI) hosted by apatite, clinopyroxene (cpx), amphibole, haüyne, and magnetite and composition of interstitial glass from alkaline gabbroic xenolith from La Palma. Prehistoric phonolites from Hernandéz-Pacheco and De La Nuez (1983)

glasses indicate an oxidation state at 2–2.5 log unit above the Ni–NiO buffer, in agreement with the crystallization of S-rich apatite and haüyne.

Chlorine concentrations in glass inclusions and interstitial glass range from 0.15 to 0.44 wt% Cl. Cl solubility is known to vary with the peraluminous-peralkaline character of the silicate glass (Carroll and Webster 1994; Webster et al. 1997), but we observed no correlation of Cl with major element concentrations or with the aluminum saturation index. Glass inclusions in clinopyroxene and apatite have Al/(Ca + Na + K) and Na/(Na + K) ratios close to those of experimental glasses used in volatile solubility experiments performed with Vesuvius phonolite by Webster et al. (2003). Comparison of the Cl contents of glass inclusions with volatile solubility data in phonolitic melts coexisting with H_2O–Cl-bearing fluids (Fig. 8) shows that the phonolitic glass inclusions were not Cl-saturated in the range 800–1000°C and 50–200 MPa.

Fig. 7 Variation of S with H_2O content of glass inclusions (GI) hosted by apatite, clinopyroxene (cpx), amphibole, haüyne and magnetite and composition of interstitial glass from alkaline gabbroic xenolith from La Palma. *Trend lines* are S solubility curves at oxidized conditions (NNO + 3.6 − 4) from water-saturated experiments with trachyandesitic compositions (*dotted lines*, 400 and 200 MPa; Luhr 1990) and fluid-saturated experiments ($XH_2O_{in} = H_2O/(H_2O + CO_2) = 1$ to 0.3, P = 400 MPa) with andesitic compositions (*black lines*; Parat et al. 2008)
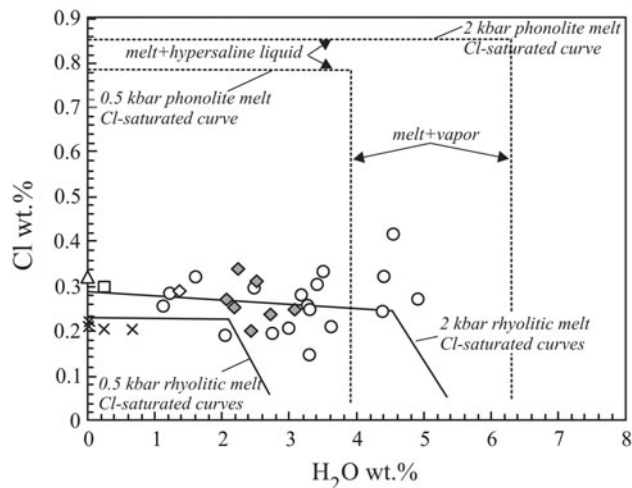

Fig. 8 Variation of Cl with H_2O content of glass inclusions hosted by apatite, clinopyroxene, amphibole, haüyne and magnetite and composition of interstitial glass from alkaline gabbroic xenolith from La Palma. *Trend lines* are Cl solubility curves at oxidized conditions (NNO + 3.6) from fluid-saturated experiments with rhyolitic and phonolitic compositions (Webster 1992; 1997; Webster et al. 2003). *Symbols* as in Fig. 7

Although experimental works have shown that S and Cl solubility are related to each other (Botcharnikov et al. 2004; Webster et al. 2009a), there is no obvious correlation between the S and Cl concentrations in glass inclusions, but Cl/S ratios vary from 2 to 16.

The fluorine content of glass inclusions and of interstitial glasses ranges from 0.07 to 0.65 wt% (Tables 1, 2) approaching the detection limit of the microprobe.

Partitioning of volatiles between glass and apatite

Tests for equilibrium between minerals and melt usually rely on exchange coefficients that can be more or less dependent on temperature and pressure. For apatite, there is no reliable exchange coefficient to check for apatite–melt equilibrium. The similar compositions of glass inclusions in apatite and clinopyroxene, however, suggest that no post-entrapment crystallization had occurred. Furthermore, compositional profiles in apatite (rim-core-rim) and in the vicinity of glass inclusions show an abrupt change in sulfur and chlorine content at the contact between apatite and glass inclusion indicating that no significant diffusive re-equilibration did occur. To estimate the sulfur, chlorine, and fluorine partition coefficients between apatite and glass inclusion, analyses of apatite were made close to the glass inclusion. Results are presented in Table 1 and Figs. 9 and 10. The OH partitioning between apatite and melt is not discussed in this study because any calculation of $D_{OH}^{apatite/melt}$ would be affected by a large uncertainty range because (1) the concentration of OH in apatite was not determined (OH could only be recalculated assuming that the halogen site in apatite is filled by Cl, F, and OH and that F + Cl + OH = 1), (2) the total H_2O concentration in glasses varies strongly (water may have been lost during degassing), and (3) it is not clear whether $D_{OH}^{apatite/melt}$ should be calculated following Boyce and Hervig (2009; $D_{OH}^{apatite/melt}$ = OH concentration in apatite/H_2O concentration in melt) or assuming only the OH concentration in melt (neglecting molecular water).

Partitioning of sulfur between apatite and glass

The sulfur content of the analyzed apatite-hosted glass inclusion ranges from 0.46 to 0.80 wt% SO_3 and broadly correlates with that of their trachytic glass inclusions (0.06 to 0.23 wt% SO_3). The partitioning is close to that observed in phase equilibria experimental works using rhyolitic and andesitic systems (0.45–0.70 wt% SO_3 in apatite for 0.03–0.30 wt% SO_3 in silicate glass) (Parat and Holtz 2004; 2005; Parat et al. 2008) (Fig. 9), suggesting that melt composition has no strong effect on the sulfur partitioning (e.g., silica activity, alkalinity). The sulfur partition coefficient determined from the composition of apatite–melt inclusion pairs ranges from 9.1 to 2.9 (Table 1). The partitioning of S does not follow Henry's Law, but decreases with increasing SO_3 in glass inclusions ($SO_{3\ glass}$ = 0.06 to 0.23 wt%), in agreement with previous experimental data.
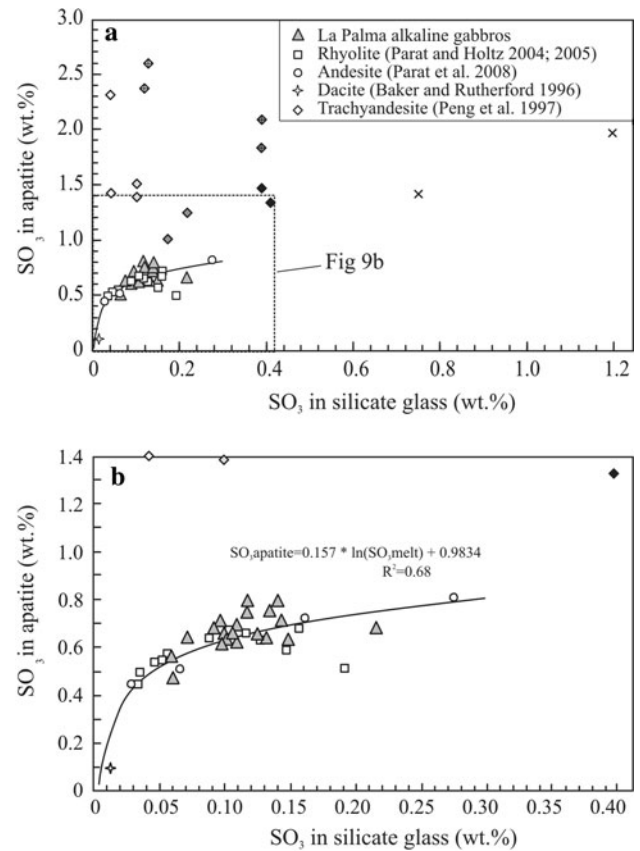

Fig. 9 Sulfur content in the silicate glass vs. sulfur content in apatite in alkaline gabbros and phase equilibria experiments. Diamonds are for experiments with trachytic composition (Peng et al. 1997) at 950, 900, 850 and 800°C and 200 and 400 MPa. Crosses are sulfur solubilities in melt at 1000°C vs. sulfur in apatite at 900 and 950°C from Luhr (1990) and Peng et al. (1997). *Squares* are for experiments with rhyolite at 900–1000°C and 200 MPa (Parat and Holtz 2004; 2005). Circles are for experiments with andesite at 850–950°C and 400 MPa (Parat et al. 2008). Star is for experiment with dacite at 760°C and 200 MPa (Baker and Rutherford 1996)

It should be noted that the sulfur partition coefficient between apatite and dacitic melt (Baker and Rutherford 1996), the only published value for very low S contents so far, does not plot on our calculated fitting curve. The reason for this discrepancy is not clear. Assuming that melt composition does not affect significantly the partitioning of sulfur, a possible explanation may be due to the high uncertainty in the determination of the low S contents in the dacite melt. The partitioning of sulfur between apatite and melt was first investigated experimentally by Peng et al. (1997). They showed that sulfur partitioning is strongly dependent on temperature and pressure, whereas for oxidized conditions (NNO + 3.7 to NNO + 4.5), the oxygen fugacity is not an important parameter. The sulfur contents in apatite reported by Peng et al. (1997) are, however, very high compared to the sulfur contents reported in more recent experimental works (Parat and

Holtz 2004; 2005; Parat et al. 2008) (Fig. 9) as well as in natural S-rich apatites (e.g., Luhr et al. 1984; Pallister et al. 1996; Streck and Dilles 1998; Tepper and Kuehner 1999; Parat et al. 2002). As noted by Peng et al. (1997) and discussed in Parat and Holtz (2004), the high sulfur content in apatites as well as sulfur zonation observed by Peng et al. (1997) may be due to kinetic effects, especially in runs performed at low temperature (800°C). Thus, these data need to be interpreted with caution. In Fig. 9a, the sulfur contents in apatite from the experiments performed at higher temperatures (900°C and 950°C, temperatures at which experiments are better suited to reach near equilibrium conditions) have been reported versus sulfur solubility at 1000°C. These points (crosses in Fig. 9a) are in good general agreement with andesitic and rhyolitic experimental data as well as data from natural samples. The partition coefficients estimated for T = 900–1000°C range from 2 to 1.7 for SO_3 melt = 0.7 to 1.3 wt% at 200 and 400 MPa, respectively and confirm the decrease of $D_S^{apatite/melt}$ toward a value of 2 with decreasing S content in melt.

Another explanation for the unusually high sulfur content (up to 2.3 wt%) in apatites analyzed by Peng et al. (1997) may be related to the source of sulfur in the experiments (performed by Luhr (1990)). Anhydrite was used for sulfur-bearing experiments at oxidizing conditions. A rapid crystallization of apatite close to anhydrite and different diffusivities for apatite-forming elements may explain the high S concentration in apatite. Problems related to different diffusivities of S, Ca, and P in the melt are expected to be particularly critical in the low-temperature experiments (e.g., 800 and 850°C), where equilibrium may not have been reached due to low diffusivities. Except for the work from Luhr (1990), other experimental works (with S added as elemental S) were not able to reproduce the high S content observed in some natural apatites (1 to 2 wt% SO_3, e.g., Parat et al. 2002; Streck et al. 2007). This suggests that a close association of sulfate and apatite may be a pre-requisite for the crystallization of S-rich apatite. This is in good agreement with evidence for co-nucleation and mutual inclusions of anhydrite and S-rich apatite in pumices from e.g., the El Chichón 1982 and the Mount Pinatubo 1991 eruptions (Luhr 2008) and haüyne and S-rich apatite in La Palma xenoliths.

Considering natural data from this study and the available experimental data from Baker and Rutherford (1996), Parat and Holtz (2004; 2005), and Parat et al. (2008), the S partitioning between apatite and glass can be expressed as:

$$SO_{3\,apatite}(wt\%) = 0.157 * \ln SO_{3\,glass}(wt\%) + 0.9834\ (r^2 = 0.68).$$

Although we did not find an influence of T, P and melt composition on the sulfur partitioning between apatite and

melt, it is emphasized that for a given fS_2, the S content in silicate glasses is a function of temperature, pressure, oxygen fugacity, and silicate glass compositions (e.g., Luhr 1990; Ducea et al. 1994; Clemente et al. 2004; Parat et al. 2008; Webster et al. 2009a), and the range of S partition coefficients ($D_S^{apatite/glass}$) may reflect some influence of these intensive parameters.

Partitioning of halogens between apatite and glass

The chlorine contents in both apatite and glass inclusions are low (0.16–0.31 wt% and 0.15–0.44 wt%, respectively, Fig. 10) and do not show a clear correlation. The partition coefficient $D_{Cl}^{apatite/glass}$ ranges from 0.4 to 1.3 (average $D_{Cl}^{apatite/glass}$ = 0.8). This range is consistent with the results of experimental research in mafic and rhyolitic systems with low Cl concentration in apatite and glass (Mathez and Webster 2005; Webster et al. 2009b).
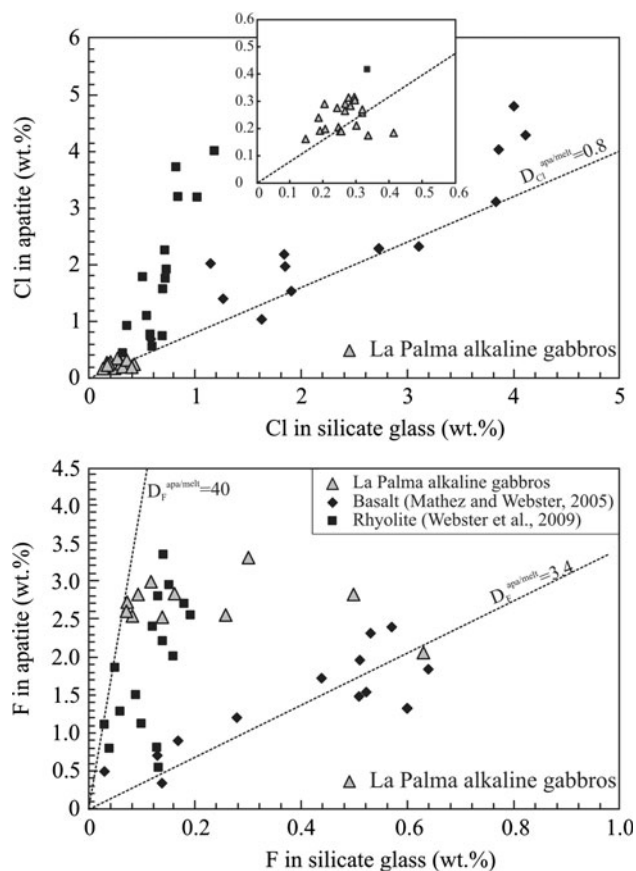

Fig. 10 Halogen content in glass inclusion vs. halogen content in hosted apatite in alkaline gabbroic xenolith from La Palma. Diamonds and squares are halogen content in melt and apatite from experimental runs (oxidized conditions, 200 MPa, 900–1100°C) with basaltic (Mathez and Webster 2005) and rhyolitic composition (Webster et al. 2009b), respectively

F content in apatite shows little variation (except one data with 2 wt% F), whereas the F content in glass inclusions ranges from 0.07 to 0.65 wt%. (Fig. 10, Table 1). Because of the very low F content in melt inclusions (close to the detection limit of 0.1 wt%), it is difficult to determine accurately the partitioning of F at low concentrations. With increasing F in glass inclusions, the partition coefficient of F between apatite and glass ($D_F^{apatite/glass}$) decreases from 35 to 3. Most of our data display, however, a high partition coefficient close to $D_F^{apatite/glass}$ determined experimentally in felsic rocks (Webster et al. 2009b). We observe no correlation of $D_F^{apatite/glass}$ with either alkalinity or aluminum content of silicate glasses.

Implications for magma evolution at La Palma

Origin of melt inclusions

The glass inclusions and interstitial glass of basanite-hosted alkaline gabbroic xenoliths vary in composition from phonolite to trachyte. Phonolites are the end-member of Recent La Palma lavas (Fig. 4) and are believed to form mainly as a result of crystal fractionation (Middlemost 1972; Klügel et al. 2000; Johansen et al. 2005). The major element compositions show that interstitial glasses and some glass inclusions resemble recent phonolite melts, whereas trachytic glass inclusions (inclusions in apatite and clinopyroxene) fall far from the liquid line of descent (Figs. 4, 5). Remarkably, their compositions overlap those of inclusions and interstitial glasses commonly found in peridotite xenoliths world wide (see summary and references in Shaw (1999)). Following scenarios are possible to explain the origin of these exotic melts:

1. The trachytic melts formed by crystal fractionation at conditions different than those prevailing during the evolution of other Recent La Palma magmas. We tested this hypothesis through a series of mixing calculations involving a wide range of potential parental liquid compositions (tephrite to phonolite) and typical cumulate minerals (amphibole, clinopyroxene, plagioclase, haüyne, magnetite, apatite) as possible fractionation phases. For any parental liquids, the mass balances for major elements yielded a sum of squared residuals between calculated and analyzed daughter melts well above 10, with the residuals of Na_2O and K_2O being particularly high. We thus conclude that trachytic melt inclusions do not represent residual melts after crystal fractionation.
2. The trachytic melts formed by partial melting of cumulate minerals during heating of the xenolith. This scenario can be ruled out on the base of mixing calculations using the same cumulus phases as above, with the residuals being significantly higher than those of the first scenario.
3. The trachytic melts formed by reactions between peridotite and Si-undersaturated basaltic melts. Some glass inclusions in apatite compositionally resemble melts found in olivine– clinopyroxene-bearing reaction zones around orthopyroxene in harzburgite (Type 2 melts in Shaw and Dingwell (2008), Fig. 4), but are higher in Al_2O_3 and lower in MgO (Fig. 5). Melts which were experimentally produced by reaction of tephritic to phonolitic liquids with forsteritic olivine match the inclusion compositions even better (C. Shaw and A. Klügel, unpubl. data). The analysis of some of these melts yields low analytical totals indicating that the melts may contain significant H_2O concentrations, as also observed in the apatite-hosted inclusions investigated in this study.

We propose, therefore, that the trachytic melts observed as inclusions in apatite and clinopyroxene have formed by reaction between tephriphonolitic to phonolitic melt (probably the host melt of the cumulates) and peridotite wall-rock. This is a likely scenario if crystal fractionation beneath La Palma occurs within the mantle.

Formation of alkaline gabbroic cumulates

On the basis of clinopyroxene-melt-barometry, Klügel et al. (2005) suggest that basanitic La Palma magmas fractionate in magma pockets at 410–770 MPa (ca. 15–26 km depth), within the uppermost mantle. Here, evolved melts may locally form and react with peridotite wall-rock to produce trachytic melts. The signature of most of these melts, resulting from the interaction of mantle rocks with differentiated magmas, becomes "lost" by subsequent magma evolution and homogenization. Thus, such melt or rock compositions cannot be found at the surface, but their equivalent may be found as melt inclusions in phenocrysts. Eventually, the phenocrysts accumulated to form alkaline gabbroic cumulates, which were transported to the surface as xenoliths during a later stage. We note that intermediate to evolved melts rather than basanites were parental to the gabbroic cumulates, because of the gabbro mineral assemblage and low Mg#. It is not known whether these cumulates formed within the uppermost mantle, or within a shallower zone of temporary magma ponding at 240–470 MPa, within the lower oceanic crust, termed "underplating level" by Klügel et al. (2005) on the base of fluid-inclusion barometry. The latter scenario appears plausible, because (1) a large number of MORB-type gabbro xenoliths from the lower oceanic crust were erupted coevally with the alkaline cumulate xenoliths,

and (2) haüyne commonly occurs as a late phase of alkaline cumulates as well as a metasomatic phase of some MORB gabbros from La Palma, but only rarely in peridotitic mantle xenoliths (Klügel et al. 1999; Neumann et al. 2000).

Volatile contents of La Palma melts

The glass inclusion compositions show that magmas beneath La Palma are relatively H_2O- and S-rich but Cl-poor (compared to Cl solubility in phonolitic melts). These magmas are more likely saturated with aqueous vapor than hypersaline liquid with further crystallization or decreasing pressure (Webster et al. 2003) (Fig. 8). The higher Cl content in phonolite glass inclusions compared to basaltic glass (0.14–0.51 and 0.07–0.12 wt%, respectively; Fig. 11) probably results from both incompatible behavior of Cl during crystal fractionation and increase in chlorine solubility with increasing alkalinity of the melt (Carroll and Webster 1994). The similar Cl content observed in glass inclusions and in degassed interstitial glasses (Fig. 8) suggests that Cl may be retained in the silicate glasses during phonolitic eruptions (Carroll 2005). At fast decompression rates, Cl cannot diffuse out of the glass efficiently, whereas H_2O can (Gardner et al. 1998).

An interesting conclusion of this study is that melts with relatively high volatile concentrations, such as those analyzed as inclusions in apatite and clinopyroxene, may be present in the mantle below La Palma. Microprobe compositional profiles in apatite show a systematic increase in S content from core to rim, indicating that the sulfur content in the host melt increased during apatite crystallization. This melt, possibly resulting from the interaction between mantle rocks and differentiated magmas under oxidizing conditions was probably not saturated with haüyne and/or sulfide during apatite crystallization, in agreement with petrographic observations (e.g., interstitial haüyne). The conditions at which haüyne crystallized is difficult to constrain, considering the lack of experimental data on the stability of this mineral (stable at least up to 400 MPa, (Berndt et al. 2001; Andújar et al. 2008). However, its crystallization is favored at high oxygen fugacity, in agreement with the high oxygen fugacity estimated from sulfur speciation (NNO + 2 to NNO + 2.5).

References

Andújar J, Costa F, Martí J, Wolff JA, Carroll MR (2008) Experimental constraints on pre-eruptive conditions of phonolitic magma from the caldera-forming El Abrigo eruption, Tenerife (Canary Islands). Chem Geol 257:173–191

Baker L, Rutherford MJ (1996) Crystallization of anhydrite-bearing magmas. In: Brown M, Candela PA, Peck DL, Stephens WE, Walker RJ, Zen E-A (eds) Origin of granites and related rocks. Geological Society of America Special Paper, pp 243–250

Balcone-Boissard H, Baker DR, Villemant B, Boudon G (2009) F and Cl diffusion in phonolitic melts: Influence of the Na/K ratio. Chem Geol 263:89–98

Belkin HE, De Vivo B, Torok K, Webster JD (1998) Pre-eruptive volatile content, melt-inclusion chemistry, and microthermometry of interplinian Vesuvius lavas pre-A.D. 1631. J Volcanol Geotherm Res 82:79–95

Berndt J, Holtz F, Koepke J (2001) Experimental constraints on storage conditions in the chemically zoned phonolitic magma chamber of the Laacher See volcano. Contrib Mineral Petrol 140(4):469–486

Botcharnikov RE, Behrens H, Holtz F, Koepke J, Sato H (2004) Sulfur and chlorine solubility in Mt. Unzen rhyodacitic melt at 850°C and 200 MPa. Chem Geol 213(1–3):207–225

Botcharnikov RE, Behrens H, Holtz F (2006) Solubility and speciation of C-O-H fluids in andesitic melt at T = 1100–1300°C and P = 200 and 500 MPa. Chem Geol 229:125–143

Botcharnikov RE, Almeev R, Koepke J, Holtz F (2008) Phase relations and liquid lines of descent in hydrous ferrobasalt—Implication for the Skaergaard Intrusion and Columbia River Flood Basalts. J Petrol 49(9):1687–1727

Boyce JW, Hervig RL (2009) Apatite as a monitor of late-stage magmatic processes at Volcán Irazú, Costa Rica. Contrib Mineral Petrol 157(2):135–145

Brenan JM (1994) Kinetics of fluorine, chlorine and hydroxyl exchange in fluorapatite. Chem Geol 110:195–210

Burgisser A, Scaillet B (2007) Redox evolution of a degassing magma rising to the surface. Nature 445:194–197

Burton M, Allard P, Muré F, La Spina A (2007) Magmatic gas composition reveals the source depth of slug-driven strombolian explosive activity. Science 317:227–230

Carracedo JC, Badiola ER, Guillou H, de la Nuez J, Pérez Torrado FJ (2001) Geology and volcanology of La Palma and El Hierro, Western Canaries. Estudios Geol 57:175–273

Carroll MR (2005) Chlorine solubility in evolved alkaline magmas. Ann Geophys 48(4/5):619–631
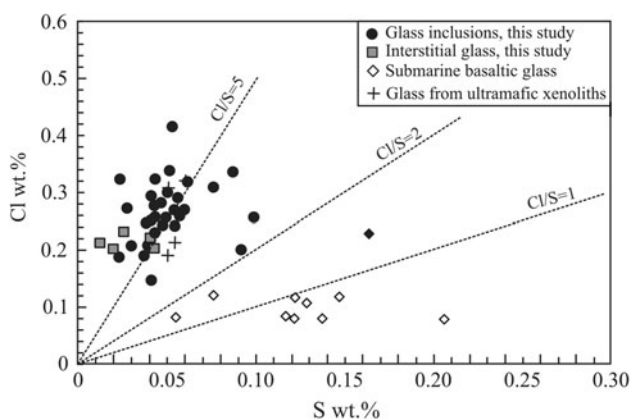

Fig. 11 Chlorine and sulfur content in glass inclusions and interstitial glasses from La Palma xenoliths (this study) and submarine basaltic glasses from la Palma (T. Hansteen, unpubl. data); Glasses from ultramafic xenoliths are from Wulff-Pedersen et al. (1996, 2000)

Carroll MR, Webster JD (1994) Solubilities of sulfur, noble gases, nitrogen, chlorine, and fluorine in magmas. In: Carroll MR, Holloway JR (eds) Volatiles in magmas. Mineralogical Society of America, Washington, DC, United States, pp 231–279

Cervantes P, Wallace PJ (2003) Magma degassing and basaltic eruption styles: a case study of 2000 year BP Xitle volcano in central Mexico. J Volcanol Geotherm Res 120:249–270

Clemente B, Scaillet B, Pichavant M (2004) The solubility of sulphur in hydrous rhyolitic melts. J Petrol 45:2171–2196

Devine JD, Gardner JE, Brack HP, Layne GD, Rutherford MJ (1995) Comparison of microanalytical methods for estimating H_2O contents of silicic volcanic glasses. Am Mineral 80:319–328

Dixon JE, Stolper EM, Holloway JR (1995) An experimental study of water and carbon dioxide solubilities in mid-ocean ridge basaltic liquids. Part I: calibration and solubility models. J Petrol 36:1607–1631

Dowty E (1980) Crystal-chemical factors affecting the mobility of ions in minerals. Am Mineral 65:174–182

Ducea MN, McInnes BIA, Wyllie PJ (1994) Sulfur variations in glasses from volcanic rocks: Effect of melt composition on sulfur solubility. Int Geol Rev 36:703–714

Gardner JE, Rutherford MJ, Hort M (1998) Degassing of trace gases during volcanic eruptions. EOS Trans AGU 79:F936

Hansteen TH, Klügel A, Schmincke HU (1998) Multi-stage magma ascent beneath the Canary Islands: evidence from fluid inclusions. Contrib Mineral Petrol 132:48–64

Hernández-Pacheco A, De la Nuez J (1983) Las extrusiones sálicas del Sur de la Isla de La Palma (Canarias). stud. Geol 39:3–30

Hernández-Pacheco A, Valls MC (1982) The historic eruptions of La Palma Island (Canarias). Arquipelago Rev Univ Azores Ser C Nat 3:83–94

Johansen TS, Hauff F, Hoernle KA, Klügel A, Kokfelt TF (2005) Basanite to phonolite differentiation within 1550–1750 year: U-Th-Ra isotopic evidence from the A.D. 1585 eruption of La Palma. Geology 33(11):897–900

Kamenetsky VS, Davidson P, Mernagh TP, Crawford AJ, Gemmell JB, Portnyagin MV, Shinjo R (2002) Fluid bubbles in melt inclusions and pillow-rim glasses: high-temperature precursors to hydrothermal fluids? Chem Geol 183:349–364

Klügel A, Schmincke HU, White JDL, Hoernle KA (1999) Chronology and volcanology of the 1949 multi-vent rift-zone eruption on La Palma (Canary Islands). J Volcanol Geotherm Res 94:267–282

Klügel A, Hoernle KA, Schmincke HU, White JDL (2000) The chemically zoned 1949 eruption on La Palma (Canary Islands): Petrologic evolution and magma supply dynamics of a rift-zone eruption. J Geophys Res 105(B3):5997–6016

Klügel A, Hansteen TH, Galipp K (2005) Magma storage and underplating beneath Cumbre Vieja volcano, La Palma (Canary Islands). Earth Planet Sci Lett 236:211–226

Koepke J (1997) Analyse von wasserhaltigen silikatischen Gläsern mit der Mikrosonde: Wassergehalte und Alkaliverluste. Beih J Mineral 9:200

Liu Y, Comodi P (1993) Some aspects of the crystal-chemistry of apatites. Mineral Mag 57:709–719

Lowenstern JB (1995) Applications of silicate melt inclusions to the study of magmatic volatiles. In: Thompson JFH (ed) Magmas, Fluids and Ore Deposits. Mineralogical Association of Canada Short Course, pp 71–99

Luhr JF (1990) Experimentally phase relations of water- and sulfur-saturated arc magmas and the 1982 eruption of El Chichón volcano. J Petrol 31:1071–1114

Luhr JF (2001) Glass inclusions and melt volatile contents at Parícutin Volcano, Mexico. Contrib Mineral Petrol 142:261–283

Luhr JF (2008) Primary igneous anhydrite: progress since its recognition in the 1982 El Chichón trachyandesite. J Volcanol Geotherm Res 175:394–407

Luhr JF, Carmichael ISE, Varekamp JC (1984) The 1982 eruptions of El Chichón volcano, Chipas, Mexico: Mineralogy and petrology of the anhydrite-bearing pumice. J Volcanol Geotherm Res 23:69–108

Marianelli P, Metrich N, Santacroce R, Sbrana A (1995) Mafic magma batches at Vesuvius: A glass inclusion approach to the modalities of feeding stratovolcanoes. Contrib Mineral Petrol 120:159–169

Mathez EA, Webster JD (2005) Partitioning behavior of chlorine and fluorine in the system apatite–silicate melt–fluid. Geochimica Cosmochimica Acta 69(5):1275–1286

Matthews SJ, Moncrieff DHS, Carroll MR (1999) Empirical calibration of the sulphur valence oxygen barometer from natural and experimental glasses; method and applications. Mineral Mag 63(3):421–431

Middlemost EAK (1972) Evolution of La Palma, Canary Archipelago. Contrib Mineral Petrol 36:33–48

Neumann ER, Sørensen VB, Simonsen SL, Johnsen K (2000) Gabbroic xenoliths from La Palma, Tenerife and Lanzarote, Canary Islands: evidence for reactions between mafic alkaline Canary Islands melts and old oceanic crust. J Volcanol Geotherm Res 103:313–342

Nikogosian IK, Elliott TR, Touret JLR (2002) Melt evolution beneath thick lithosphere; a magmatic inclusion study of La Palma, Canary Islands. Chem Geol 183:169–193

Pallister JS, Hoblitt RP, Meeker GP, Knight RJ, Siems DF (1996) Magma mixing at Mount Pinatubo; petrographic and chemical evidence from the 1991 deposits. In: Newhall CG, Punongbayan RS (eds) Fire and mud; eruptions and lahars of Mount Pinatubo, Philippines, pp 687–731

Parat F, Holtz F (2004) Sulfur partitioning between apatite and melt and effect of sulfur on apatite solubility at oxidizing conditions. Contrib Mineral Petrol 147:201–212

Parat F, Holtz F (2005) Sulfur partition coefficient between apatite and rhyolite: the role of bulk S content. Contrib Mineral Petrol 150(6):643–651

Parat F, Dungan MA, Streck MJ (2002) Anhydrite, pyrrhotite and sulfur-rich apatite: tracing the sulfur evolution of an Oligocene andesite (Eagle Mountain, Colorado, U.S.A.). Lithos 64:63–75

Parat F, Holtz F, Feig S (2008) Pre-eruptive conditions of the Huerto Andesite (Fish Canyon system, San Juan volcanic field, Colorado): Influence of volatiles (C-O-H-S) on phase equilibria and mineral composition. J Petrol 49(5):911–935

Peng G, Luhr JF, McGee JJ (1997) Factors controlling sulfur concentrations in volcanic apatite. Am Mineral 82:1210–1224

Piccoli PM, Candela PA (1994) Apatite in felsic rocks: a model for the estimation of initial halogen concentrations in the Bishop Tuff (Long Valley) and Tuolumne Intrusive Suite (Sierra Nevada Batholith) magmas. Am J Sci 294:92–135

Piccoli PM, Candela PA (2002) Apatite in igneous systems. Rev Mineral Geochem 48:255–292

Portnyagin M, Almeev R, Matveev S, Holtz F (2008) Experimental evidence for rapid water exchange between melt inclusions in olivine and host magma. Earth Planet Sci Lett 272:541–552

Rouse RC, Dunn PJ (1982) A contribution to the crystal chemistry of ellestadite and the silicate sulfate apatites. Am Mineral 67(1–2):90–96

Schmincke HU, Klügel A, Hansteen TH, Hoernle K, von den Bogaard P (1998) Samples from the Jurassic ocean crust beneath Gran Canaria, La Palma and Lanzarote (Canary Islands). Earth Planet Sci Lett 163:343–360

Shaw CSJ (1999) Dissolution of orthopyroxene in basanitic magma between 0.4 and 2 GPa: further implications for the origin of Si-rich alkaline glass inclusions in mantle xenoliths. Contrib Mineral Petrol 135:114–132

Shaw CSJ, Dingwell DB (2008) Experimental peridotite–melt reaction at one atmosphere: a textural and chemical study. Contrib Mineral Petrol 155:199–214

Stormer JC (1983) The effects of recalculation on estimates of temperature and oxygen fugacity from analyses of multicomponent iron-titanium oxides. Am Mineral 68:586–594

Streck MJ, Dilles JH (1998) Sulfur evolution of oxidized arc magmas as recorded in apatite from a porphyry copper batholith. Geology 26(6):523–526

Streck MJ, Wacaster S (2006) Plagioclase and pyroxene hosted melt inclusions in basaltic andesites of the current eruption of Arenal volcano, Costa Rica. J Volcanol Geotherm Res 157:236–253

Streck MJ, Broderick CA, Halter WE (2007) Origin of sulfur rich apatite in silicic, calc-alkaline magmas. Goldschmidt 2007 conference, Köln, Germany

Tepper JH, Kuehner SM (1999) Complex zoning in apatite from the Idaho Batholith; a record of magma mixing and intracrystalline trace element diffusion. Am Mineral 84(4):581–595

Toulmin P, Barton PB (1964) A thermodynamic study of pyrite and pyrrhotite. Geochim Cosmochim Acta 28:641–671

Vaggelli G, De Vivo B, Trigila R (1993) Silicate-melt inclusions in recent Vesuvius lavas (1631–1944): II. Analytical chemistry. J Volcanol Geotherm Res 58:367–376

Webster JD (1992) Fluid-melt interactions involving Cl-rich granites: Experimental study from 2 to 8 kbar. Geochimica Cosmochimica Acta 56:659–678

Webster JD (1997) Chloride solubility in felsic melts and the role of chloride in magmatic degassing. J Petrol 38(12):1793–1807

Webster JD, Thomas R, Rhede D, Förster H, Seltmann R (1997) Melt inclusions in quartz from an evolved peraluminous pegmatite: geochemical evidence for a strong tin enrichment in fluorine-rich and phosphorus-rich residual liquids. Geochimica Cosmochimica Acta 61:2589–2604

Webster JD, De Vivo B, Tappen CM (2003) Volatiles, magmatic degassing and eruptions of the Mt. Somma-Vesuvius: Constrains from silicate melt inclusions, Cl and H_2O solubility experiments and modeling. In: De Vivo B, Bodnar RJ (eds) Melt Inclusions in Volcanic Systems: Methods, Applications and Problems, pp 207–226

Webster JD, Sintini MF, De Vivo B (2009a) The partitioning behavior of Cl, S, and H_2O in aqueous vapor- $\pm$ saline-liquid saturated phonolitic and trachytic melts at 200 MPa. Chem Geol 263:19–36

Webster JD, Tappen CM, Mandeville CW (2009b) Partitioning behavior of chlorine and fluorine in the system apatite-melt-fluid. II: Felsic silicate systems at 200 MPa. Geochimica Cosmochimica Acta 73:559–581

Wulff-Petersen E, Neumann E-R, Jensen BB (1996) The upper mantle under La Palma, Canary Islands: formation of Si-K-Na-rich melt and its importance as a metasomatic agent. Contrib Mineral Petrol 125:113–139

Wulff-Petersen E, Neumann E-R, Burke EAJ, Vannucci RPB, Ottolini L, Gjonnes J, Hansen V (2000) Origin and structural character of haüyne$_{ss}$ in spinel dunite xenoliths from La Palma, Canary Islands. Am Mineral 85:1397–1405